RSC Advances

PAPER

View Article Online
View Journal | View Issue

Cite this: *RSC Adv.*, 2018, **8**, 2873

"Turn on" room-temperature phosphorescent biosensors for detection of hyaluronic acid based on manganese-doped ZnS quantum dots†

Dongxia Li, Jin Qin, Jinzhi Lv, Jiajia Yang and Guiqin Yan *

Biosensors based on excellent optical properties of quantum dots (QDs) nanohybrids are efficient for biological detection. In this work, a room-temperature phosphorescent (RTP) PDAD–Mn–ZnS QDs biosensor was constructed with poly(diallyldimethylammonium chloride) (PDAD) as the modifier of MPA-capped Mn–ZnS QDs, and used to detect hyaluronic acid (HA). The newly-added HA induced severe electrostatic interaction with PDAD–Mn–ZnS QDs, leading to the aggregation between PDAD–Mn–ZnS QDs and HA and thereby enhancing RTP. The enhancement of RTP was proportional to the HA concentrations within certain ranges. On this basis, a high-performance HA sensor was built and this sensor had a detection limit of 0.03 μg mL^{-1} and a detection range of 0.08–2.8 μg mL^{-1}. This proposed RTP sensor can avoid interferences from the background fluorescence or scattering light of the matrix that are encountered in spectrofluorometry. Thus, this biosensor is potentially suitable for detection of HA in real samples without complicated pretreatment.

Received 27th October 2017
Accepted 8th January 2018

DOI: 10.1039/c7ra11858a

rsc.li/rsc-advances

1. Introduction

Hyaluronic acid (HA) is a negatively-charged glycosaminoglycan composed of glycuronic acid-*N*-acetylglucosamine as disaccharide units.[1–3] HA is ubiquitous in various tissues and organs and is a major component of extracellular matrix.[4–6] Research proves HA is closely associated with the survival, migration, occurrence and angiogenesis of tumor cells, and the HA concentrations are higher in malignant tumors than in benign tumors and normal cells.[7–11] Clinical data suggest serum HA concentrations increase after the occurrence of hepatocirrhosis, liver fibrosis or rheumatism.[12–14] Thus, quantitative detection of HA concentrations in serum or tissues is valuable for diagnosis and prognosis of diseases. Moreover, HA have outstanding rheological properties that make it an attractive biomaterial.[15,16] It has been widely applied in medicine,[15–18] cosmetics[19,20] and other fields. Thus, researchers have to establish specific methods for rapidly controlling and sensitively detecting HA in complicated samples.

So far, there many effective methods for this purpose, such as carbazole assay,[21] enzyme-linked immunosorbent assay (ELISA)[11,22] and colorimetry.[23] These methods are mainly based on the hydrolysis of HA, but are limited by discontinuity, strict requirements for detection conditions, and large time consumption. To solve these limitations, some researchers have looked for alternative methods based on diverse signals of fluorescence,[24,25] Rayleigh resonance scattering (RRS),[26] turbidimetry[27,28] and high-performance liquid chromatography (HPLC).[29] Despite the improvement of sensitivity and precision, the application of these new methods is limited by the requirement of special instruments, complex sample pretreatment, and background interference. Thus, developing convenient, fast and sensitive HA detection methods is of great practical meaning. Along with the quick development of quantum dots (QDs) in biology, QDs have attracted growing attention as molecular recognition agents of biosensor development.

QDs are a novel type of semiconductor luminescent nanomaterials that outstand with optical stability, high quantum yield and narrow emission spectrum.[30–37] QDs have attracted wide attention from researchers of biomolecule detection and are extensively used to detect and analyze diverse small molecules, proteins and DNA.[33–36] Recently, room-temperature phosphorescence (RTP) QDs detection has attracted much attention.[37–41] Compared with fluorescence QDs, phosphorescent QDs survive longer, better avoid the interference from scattering and autofluorescence, and do not need complex sample pretreatment.[37,39,42] Moreover, phosphorescence is rarer than fluorescence and thus is more efficient and selective in practice.[38,39] These properties provide a new route for analysis and measurement of bioactive molecules or intracellular active substances.

In this work, by utilizing the excellent optical properties of phosphorescent Mn–ZnS QDs, we designed a simple phosphorescent sensor for HA detection. The designing principle is

Shanxi Normal University, Linfen 041004, PR China. E-mail: gqyan2013@163.com; Fax: +86-357-2051249

† Electronic supplementary information (ESI) available. See DOI: 10.1039/c7ra11858a

illustrated in Fig. 1. A cationic chain-typed poly(-diallyldimethylammonium chloride) (PDAD) was selected as the modifier of MPA-capped Mn–ZnS QDs to form QDs nanohybrids with surface positive charge. After addition HA, HA as an anionic mucopolysaccharide could induce severe electrostatic interaction with PDAD–Mn–ZnS QDs, leading to QDs aggregation and an enhancement of QDs room-temperature phosphorescence (RTP). This method can effectively avoid the interference from the background fluorescence of biological samples. Thus, it can rapidly, accurately, and easily detect the HA in biological samples.

2. Experimental

2.1 Materials and chemicals

Mercaptopropionic acid (MPA, J&K Chemical Co. Ltd., China), $Zn(Ac)_2 \cdot 2H_2O$, $Mn(Ac)_2 \cdot 4H_2O$ and $Na_2S \cdot 9H_2O$ (Tianjin Kemiou Chemical Reagent Co. Ltd., China) were used to prepare MPA-capped Mn-doped ZnS QDs. Other materials and chemicals included poly(diallyldimethylammonium chloride) (PDAD), hyaluronic acid sodium salt (HA), bovine serum albumin (BSA) (Aladdin Bio-Chem Technology Co. Ltd., Shanghai, China), human serum albumin (HSA, Sigma-Aldrich, USA), and human serum samples (Chongqing Manuik Technology Co. Ltd., China). Ultrapure water (18.2 MΩ cm) produced by a Water Pro water purification system (Labconco, USA) was used to prepare all the solutions.

2.2 Apparatuses

The morphology and microstructure of QDs were characterized by a JEM-2100F transmission electron microscope (TEM, Japan). The crystalline structure of QDs was studied by a D/Max-2500 powder X-ray diffractometer (XRD, Rigaku, Japan). Ultraviolet (UV) spectra were measured on a UV-29100 ultraviolet/visible (UV/vis) spectrophotometer (Shimadzu, Japan). Resonance light scattering (RLS) spectra were recorded on the same spectrofluorometer by simultaneous scanning of excitation and emission monochromators ($\Delta l = 0$) from 200 to 700 nm. Phosphorescence was measured by a Cary Eclipse fluorescence spectrophotometer (Varian, USA) equipped with a plotter unit and a quartz cell (1×1 cm^2) in the phosphorescence mode. In addition, zeta potential was measured by a ZS90 Zetasizer Nanoscale device, and pH was tested by a pH meter (Jinpeng Analytical Instruments, China).

2.3 Synthesis of MPA-capped Mn-doped ZnS QDs

MPA-capped Mn-doped ZnS QDs were synthesized according to a reported method[37,39] with some modification. Briefly, 50 mL of 0.04 M MPA, 5 mL of 0.1 M $Zn(Ac)_2$ and 2 mL of 0.01 M $Mn(Ac)_2$ were added to a three-necked bottle. The resulting solution was adjusted to pH 11 by adding 1 M NaOH and magnetically stirred at room temperature and nitrogen protection for 30 min. Then 5 mL of 0.1 M Na_2S was added for 20 min of reaction. The resulting QDs were aged at 50 °C in open air for 2 h, precipitated in an equal volume of anhydrous ethanol, and centrifuged at high speed. After the supernatant was discarded, the precipitates were washed by ethanol three times. The final powder QDs were vacuum-dried at room temperature for 24 h and prefabricated.

2.4 Preparation of PDAD–Mn–ZnS QDs

The PDAD–Mn–ZnS QDs were prepared according to a reported method[36,43] with some modification. First, the Mn–ZnS QDs were dissolved in ultrapure water, followed by addition of 0.35 wt% PDAD and stirred for 10 min. The mixed solution was added with a same volume of ethanol and then centrifuged. After the resulting supernatant was discarded, the precipitates

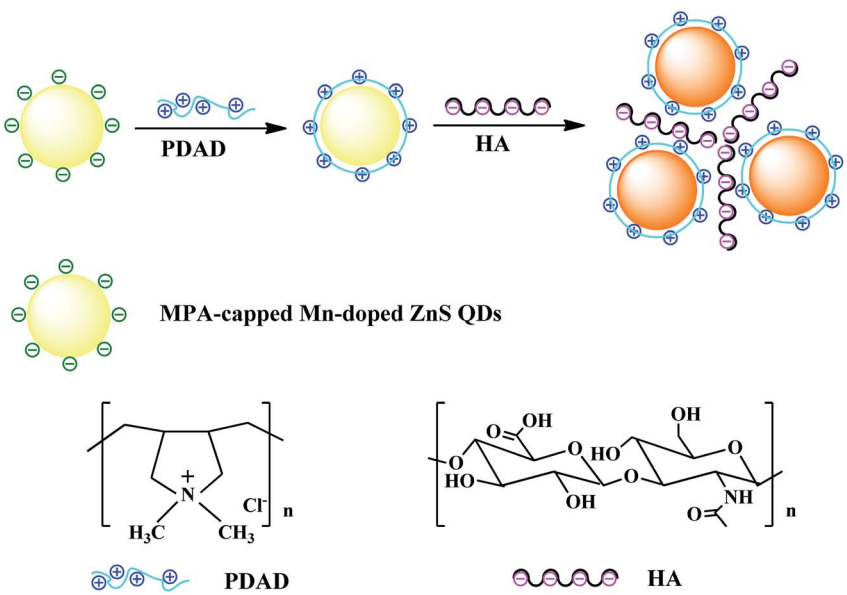

Fig. 1 Schematic illustration of fabricating of PDAD–Mn–ZnS QDs for HA detection.

were washed again with anhydrous ethanol and centrifuged. The resulting solution was diluted in a phosphate buffer solution (PBS, pH 7.4, 0.02 M). Finally, a 1.0 mg mL^{-1} PDAD–Mn–ZnS QDs solution was prepared.

2.5 Performance of HA detection

To study the effects of HA on the RTP of PDAD–Mn–ZnS QDs, we prepared a 0.1 mg mL^{-1} HA water solution and a 1.0 mg mL^{-1} PDAD–Mn–ZnS QDs solution. Then to several 10 mL colorimetric tubes, 500 μL of phosphate buffer solution (PBS, pH 7.4, 0.2 M), 50 μL of the PDAD–Mn–ZnS QDs solution, and different volumes of the HA solution were added successively. The tubes were shaken uniformly and added with water to 5 mL. After 15 min, RTP in each tube was detected at the excitation wavelength of 295 nm.

2.6 Sample pretreatment

Sodium hyaluronate eye drops (1 mg mL^{-1}, Qilu Pharmaceutical Co. Ltd., China) were dissolved in the phosphate buffer (pH 7.4, 0.2 M) to obtain a solution of 10 μg mL^{-1}. Human serum samples were diluted 100 times for analysis. No further complex pretreatment procedures were needed in the sample preparation.

2.7 Sample detection

To 10 mL colorimetric tubes, PBS (500 μL pH 7.4, 0.2 M), PDAD–Mn–ZnS QDs (50 μL, 1 mg mL^{-1}), sodium hyaluronate eye drops (200 μL) or human serum sample (50 μL) were successively added. The mixture solutions were all diluted with ultrapure water to 5 mL and were shaken uniformly. After 15 min, RTP in each tube was detected at the excitation wavelength of 295 nm. The spiked quantities of HA were 1.2 and 2.0 μg mL^{-1}. All experiments were conducted in triplicate. The samples were diluted 100 times, without any other pretreatment.

3. Results and discussion

3.1 Characterizations of MPA-capped Mn–ZnS QDs and PDAD–Mn–ZnS QDs

The shape and size of the MPA-capped Mn–ZnS QDs were characterized by TEM (Fig. S1A†). The MPA-capped Mn–ZnS QDs look like uniform near-spherical particles, with the size of ~4 nm (Fig. S1B†). XRD shows the Mn–ZnS QDs have three obvious diffraction peaks, corresponding to the crystal faces (111), (220) and (311) of cubic ZnS (Fig. S2†). It is indicated the newly-prepared Mn–ZnS QDs have a typical cubic crystal structure, which is consistent with a previous study.[44] These results confirm the successful synthesis of MPA-capped Mn–ZnS QDs. PDAD with significant positive charge was used as a positively-charged modifier of the QDs. PDAD would bind onto the surfaces of the MPA-capped Mn–ZnS QDs through electrostatic interaction, forming the positively-charged the PDAD–Mn–ZnS QDs. Fig. S3† shows the TEM images of the PDAD–Mn–ZnS QDs.

Further characterizations of their optical properties are showed in Fig. 2. These Mn–ZnS QDs have the maximum absorption peak at 295 nm (curve a) and maximum emission peak at 590 nm (curve b). This RTP of Mn–ZnS QDs was induced by the transition of electrons from the emission triplet state $^4T_1$ to the $^6A_1$ ground state.[45] First ZnS was excited, so the excited state electrons were captured by the cavity Mn^{2+}, and then the electrons and holes formed a compound on Mn^{2+}, exciting Mn^{2+} and finally releasing energy in the form of RTP.[46] As showed in Fig. 2, PDAD–Mn–ZnS QDs have nearly the same absorption peak at 295 nm (curve a and curve c) as Mn–ZnS QDs, indicating PDAD bonded to the surfaces of Mn–ZnS QDs and did not change the absorptive properties of Mn–ZnS QDs. Moreover, the PDAD–Mn–ZnS QDs and Mn–ZnS QDs nearly have the same emission spectra at room temperature, with an emission peak appears at 590 nm (curve b and curve d), except that the phosphorescence intensity of PDAD–Mn–ZnS QDs is only slightly enhanced. The relative positions of the excitation and emission spectra were basically not changed after modification by PDAD, indicating the variation of surface modifying groups did not alter the properties of QDs.[39]

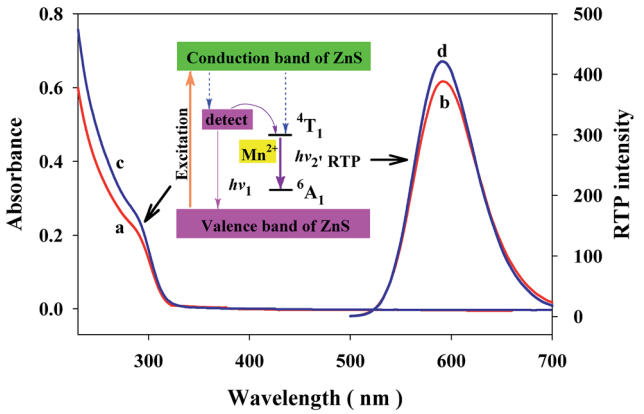

Fig. 2 UV/vis spectra (curves a and c) and RTP emission spectra (curves b and d) of Mn–ZnS QDs (10 μg mL^{-1}; curves a and b), and PDAD–Mn–ZnS QDs (10 μg mL^{-1}; curves c and d).

3.2 HA detection based on RTP of PDAD–Mn–ZnS QDs

To investigate the feasibility of using the RTP of PDAD–Mn–ZnS QDs into HA detection, we studied how HA concentrations would affect the RTP intensity of PDAD–Mn–ZnS QDs. Fig. 3A shows that the RTP intensity at 590 nm of PDAD–Mn–ZnS QDs is gradually strengthened with the rise of HA concentration. Fig. 3B shows at the HA concentration of 2.8 μg mL^{-1}, the RTP intensity of PDAD–Mn–ZnS QDs basically stabilizes. This phenomenon suggests the HA concentration largely affects the RTP intensity of PDAD–Mn–ZnS QDs. In this case, it is possible to build a sensitive HA detection method.

3.3 Optimization of experimental conditions

The pH and reaction time of the detection system are closely associated with the stability and selectivity of the sensor. Fig. S4† shows how pH and reaction time affect the RTP intensity of PDAD–Mn–ZnS QDs. Clearly, pH is an important influence factor on system stability. As showed in Fig. S4A,† the RTP intensity of PDAD–Mn–ZnS QDs is gradually strengthened

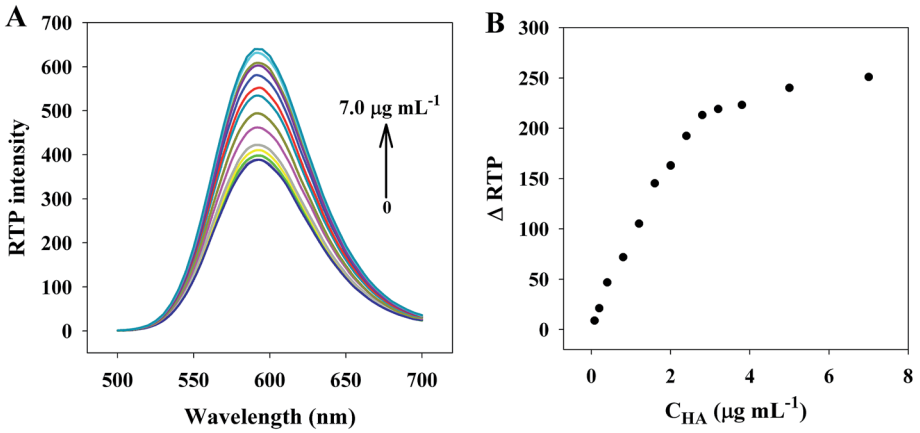

Fig. 3 (A) HA concentration-dependent RTP emission spectra of PDAD–Mn–ZnS QDs. (B) The plot of ΔRTP intensity with the increase of the concentration of HA. Buffer, 20 mM PBS (pH, 7.4); PDAD–Mn–ZnS QDs, 10 μg mL^{-1}.

with the rise of pH within pH = 5.6–8.5, but is relatively stable within pH 7.0–8.0. Since the pH of biological fluids is 7.35–7.45, we selected pH 7.4 as the optimal pH of this sensor and used it in the subsequent experiments. Then, the effect of time on the RTP intensity of the PDAD–Mn–ZnS QDs/HA system is studied. Fig. S4B† shows the RTP intensity of PDAD–Mn–ZnS QDs basically stabilizes within 60 min. Thus, to ensure sufficient reaction between PDAD–Mn–ZnS QDs and HA, we set the reaction time at 15 min.

3.4 Calibration curves and sensitivity

As showed in Fig. 4A, at the optimal conditions, we built an RTP HA detection sensor based on PDAD–Mn–ZnS QDs. This sensor had a linear detection range of 0.08–2.8 μg mL^{-1}, with a linear equation $\Delta RTP = 78.946C_{HA} + 9.8331$ ($R = 0.995$). Moreover, its detection limit is 0.03 μg mL^{-1}. Specifically, σ is the standard deviation of phosphorescence intensity after parallel measurement with the 0.2 μg mL^{-1} HA solution. The relative standard deviation of 11 parallel measurements is 2.1%.

As showed in Table 1, the detection limit of the RTP method is lower than RRS,[26] turbidimetry[27] and HPLC-UV,[29] but is higher than fluorescent assay[25] methods. Unlike fluorescence methods, RTP methods are less interfered by the background fluorescence of biological fluids. Fig. 4B only uncovers strong background fluorescence, but no background phosphorescence in human serum. Thus, our new method is feasible for detection of target molecules in biological fluids, so the samples can be detected directly only after dilution, which simplifies the analytical procedures and further stabilizes the detection performance.

3.5 Mechanism of PDAD–Mn–ZnS QDs in HA detection

UV/vis absorption results (Fig. 5A) shows the PDAD–Mn–ZnS QDs have obvious UV absorption at 240–360 nm, HA shows no evident UV absorption at 240–360 nm, while the UV absorption is significantly weakened after the interaction between PDAD–Mn–ZnS QDs and HA, indicating HA could modestly interact with PDAD–Mn–ZnS QDs.

The scattering particles formed from the electrostatic interaction of these two substances will produce RLS signals. RLS analysis (Fig. 5B) shows the RLS intensity of PDAD–Mn–ZnS QDs alone is very weak within 200–700 nm, but after the addition of HA, it is gradually strengthened with the increase of HA

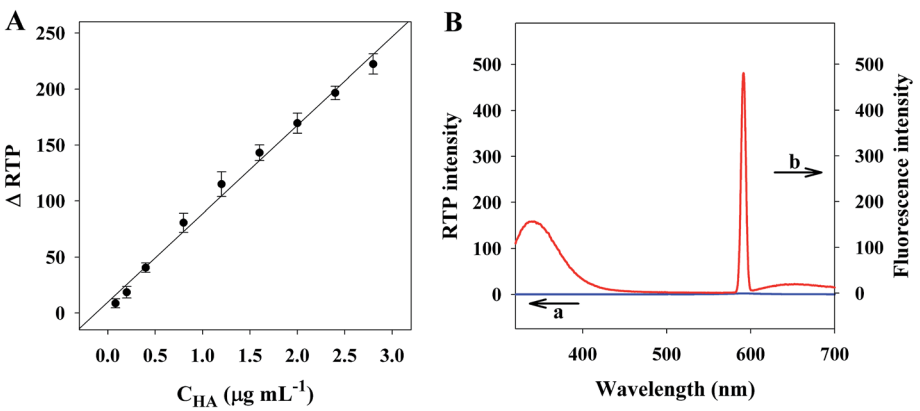

Fig. 4 (A) Plots of ΔRTP as a function of HA concentration show a linear range; (B) RTP spectra (curve a) and fluorescence spectra (curve b) of human serum. Buffer, 20 mM PBS (pH, 7.4); PDAD–Mn–ZnS QDs, 10 μg mL^{-1}.

Table 1 Comparison of the proposed method with different analytical techniques reported for detection of HA

Methods	Detection range (μg mL $^{-1}$)	LOD (μg mL^{-1})	Reference
Fluorescent assay	0.2 × 10^{-3} to 0.5	0.2 × 10^{-3}	25
Rayleigh resonance scattering	0.4–48.0	0.096	26
CTAB turbidimetric method	20–160	1.55	28
HPLC-UV	320–480	—	29
Phosphorescence based on QDs	0.08–2.8	0.03	This work

concentration, indicating PDAD–Mn–ZnS QDs and HA aggregate during the interaction process to form larger scattering particles.

Then high-concentration NaCl solution could interfere with the RLS of the PDAD–Mn–ZnS QDs/HA system, indicating the major causes for the aggregation between PDAD–Mn–ZnS QDs and HA is electrostatic attraction (Fig. 5C). The RLS intensity of the PDAD–Mn–ZnS QDs/HA system is significantly reduced by the high salt ionic strength. This is because with the increase of ion concentration, anions are adsorbed onto the surface of the positively-charged PDAD–Mn–ZnS QDs to neutralize the surface positive charge, thereby inhibiting the electrostatic interaction between PDAD–Mn–ZnS QDs and HA and reducing the RLS intensity. Fig. S5† shows the TEM images of the PDAD–Mn–ZnS QDs/HA that comparison with the TEM of PDAD–Mn–ZnS QDs proved the addition of HA significantly induced the aggregation of PDAD–Mn–ZnS QDs.

The zeta potential analysis (Fig. 5D) shows the potentials of PDAD–Mn–ZnS QDs solution and the HA solution at pH 7.4 are +31.7 and −41.5, respectively. After the mixing, the potential changes to +7.2. These results further confirm electrostatic interaction is responsible for the aggregation between PDAD–Mn–ZnS QDs and HA.

The optical properties of QDs are closely related with their surface status. After the addition of HA into the PDAD–Mn–ZnS QDs solution, the interaction between them induced the aggregation of PDAD–Mn–ZnS QDs, shortening the distances between PDAD–Mn–ZnS QDs and enhancing the Coulomb force of QDs. As a result, the local electric field around QDs was strengthened, which induced more efficient stimulation from

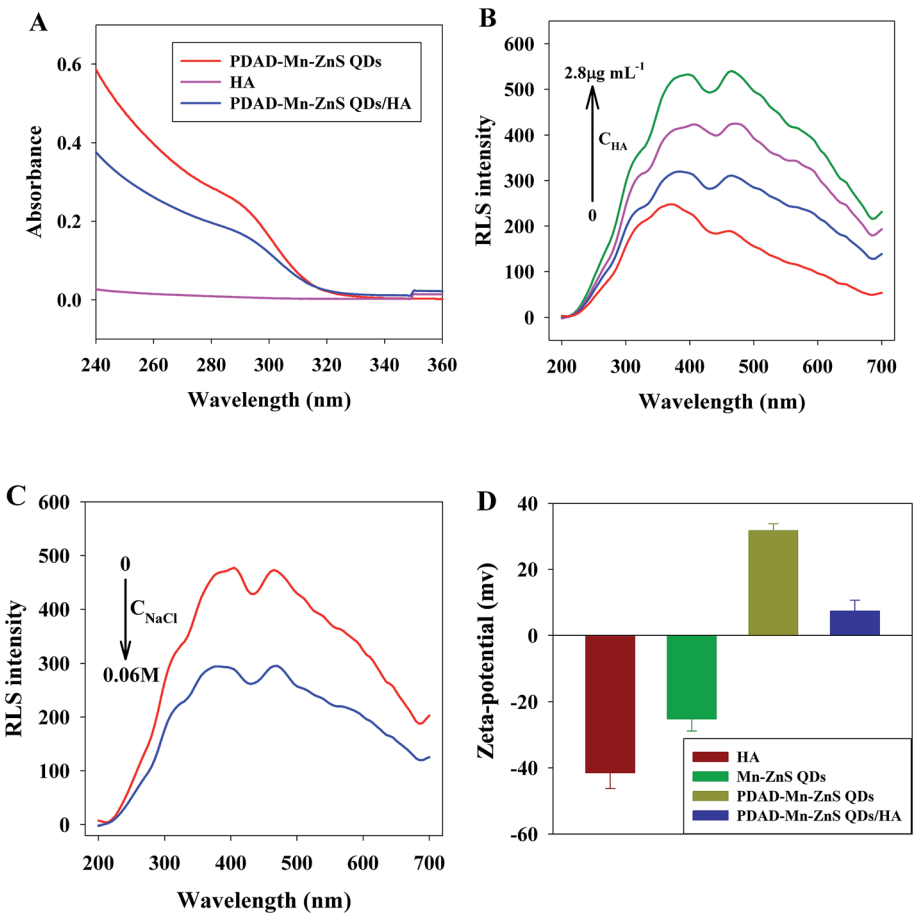

Fig. 5 (A) UV-vis absorption spectra of PDAD–Mn–ZnS QDs, HA, PDAD–Mn–ZnS QDs/HA. (B) Changes of the PDAD–Mn–ZnS QDs RLS after addition of HA. (C) Changes of the PDAD–Mn–ZnS QDs/HA RLS after addition of NaCl. (D) The zeta potential histogram of Mn–ZnS QDs, PDAD–Mn–ZnS QDs, HA and PDAD–Mn–ZnS QDs/HA. The concentration of Mn–ZnS QDs, PDAD–Mn–ZnS QDs and HA was 10 μg mL^{-1}, 10 μg mL^{-1} and 2.8 μg mL^{-1}, respectively.

Table 2 Recovery for the determination of HA in real samples (mean ± s; $n = 3$)

Type of samples	Spiked (μg mL^{-1})	RSD (%)	Recovery (%)
Sodium hyaluronate eye drops	1.2	1.7	97.9
	2.0	2.9	103.1
Human serum	1.2	2.5	106.8
	2.0	3.4	98.7

QDs. Thereby, more energy was transited from the surfaces of QDs to Mn^{2+}, which increased the RTP intensity.[47]

3.6 Interference from foreign substances

Under optimal experimental conditions, we investigated how some common coexisting substances in human liquids would interfere with the HA detection sensor. As showed in Table S1,† at the HA concentration of 0.4 μg mL^{-1} (1 μM), the Na^+ or K^+ at tolerance ratio of 1000, Mg^{2+} or Ca^{2+} at tolerance ratio of 100, glucose at tolerance ratio of 300, arginine or cysteine at tolerance ratio of 500, or BSA, HAS, insulin, ALP or DNA at tolerance ratio of 50 nearly did not interfere with the phosphorescence intensity of the detection system. However, excessive BSA, HSA, insulin, ALP or DNA affected the phosphorescent intensity of the system. This is because the biomacromolecules BSA, HSA, insulin, ALP and DNA were negatively charged at pH 7.4 and could interact with PDAD–Mn–ZnS QDs, thereby affecting the phosphorescent intensity. But, the normal content of HSA in human serum was 30–55 mg mL^{-1} (430–793 μM). When the 100-fold diluted human serum samples were used as the medium for the evaluation, the concentration of HSA was lower than listed in the table and thus did not affect the detection system. The serum concentrations of BSA, insulin, ALP and DNA were far smaller than that of HAS, so these substances after dilution did not affect the system. These results suggest the RTP of PDAD–Mn–ZnS QDs is highly selective for HA detection.

3.7 Sample analysis

To investigate the real application performance of the RTP sensor in HA detection based on PDAD–Mn–ZnS QDs, we conducted spiked recovery trials for sodium hyaluronate eye drops and human serum samples. As showed in Table 2, the average recovery rate is 97.9–106.8%, which is satisfactory for laboratory experiments and further confirms that the PDAD–Mn–ZnS QDs RTP sensor is feasible for HA detection in real samples.

4. Conclusions

With phosphorescent QDs as a signal carrier, we built a PDAD–Mn–ZnS QDs nanohybrid, and used it as the RTP probe of HA. Then this system was used to detect HA at physiological pH. Under the optimal experimental conditions, the HA concentration within 0.08–2.8 μg mL^{-1} was well linearly correlated with the RTP intensity of the PDAD–Mn–ZnS QDs nanohybrid, with a detection limit of 0.03 μg mL^{-1}. This sensor was designed as easy and convenient operation. More importantly, when used to detect real samples, this sensor avoids the interference of autofluorescence and scattering light from the biological fluids, and does not need complex sample pretreatment. Thus, this sensor can be used to efficiently detect HA in sodium hyaluronate eye drops and human serum.

Conflicts of interest

The authors declare that there is no conflict of interest.

Acknowledgements

This work was supported by the National Natural Science Foundation of China (Grant 31700862 and 31700876), the Fund for Construction Program of Chemical Advantage and Key discipline of Shanxi Province of China (Grant 912019).

References

1 T. C. Laurent and J. R. Fraser, *FASEB J.*, 1992, **6**, 2397–2404.
2 W. Yang, J. Ni, F. Luo, W. Weng, Q. Wei, Z. Lin and G. Chen, *J. Anal. Chem.*, 2017, **89**, 8384–8390.
3 S. P. Evanko, M. I. Tammi, R. H. Tammi and T. N. Wight, *Adv. Drug Delivery Rev.*, 2007, **59**, 1351–1365.
4 K. Kouvidi, A. Berdiaki, D. Nikitovic, P. Katonis, N. Afratis, V. C. Hascall, N. K. Karamanos and G. N. Tzanakakis, *J. Biol. Chem.*, 2011, **286**, 38509–38520.
5 Y. H. Yun, D. J. Goetz, P. Yellen and W. Chen, *Biomaterials*, 2004, **25**, 147–157.
6 M. K. Cowman, H.-G. Lee, K. L. Schwertfeger, J. B. McCarthy and E. A. Turley, *Front. Immunol.*, 2015, **6**, 261.
7 R. H. Tammi, A. Kultti, V.-M. Kosma, R. Pirinen, P. Auvinen and M. I. Tammi, *Semin. Cancer Biol.*, 2008, **18**, 288–295.
8 M. P. Carvalho, E. C. Costa, S. P. Miguel and I. J. Correia, *Carbohydr. Polym.*, 2016, **150**, 139–148.
9 P. Auvinen, R. Tammi, J. Parkkinen, M. Tammi, U. Ågren, R. Johansson, P. Hirvikoski, M. Eskelinen and V.-M. Kosma, *Am. J. Pathol.*, 2000, **156**, 529–536.
10 V. Assmann, C. Fieber, P. Herrlich, M. Hofmann, C. C. Termeer, T. Ahrens and J. C. Simon, *J. Invest. Dermatol.*, 2001, **116**, 93–101.
11 R. S. Yahya, A. A. El-Bindary, H. A. El-Mezayen, H. M. Abdelmasseh and M. A. Eissa, *Clin. Lab.*, 2014, **60**, 1115–1121.
12 M. Sharif, E. George, L. Shepstone, W. Knudson, E. J. M. A. Thonar, J. Cushnaghan and P. Dieppe, *Arthritis Rheum.*, 1995, **38**, 760–767.
13 K. Aghcheli, H. Parsian, D. Qujeq, M. Talebi, A. Mosapour, E. Khalilipour, F. Islami, S. Semnani and R. Malekzadeh, *Eur. J. Intern. Med.*, 2012, **23**, 58–64.
14 H. Parsian, A. Rahimipour, M. Nouri, M. H. Somi, D. Qujeq, M. K. Fard and K. Agcheli, *J. Gastrointestin Liver Dis.*, 2010, **19**, 169–174.
15 M. E. Adams, A. J. Lussier and J. G. Peyron, *Drug Saf.*, 2000, **23**, 115–130.

16 J. Arrich, F. Piribauer, P. Mad, D. Schmid, K. Klaushofer and M. Müllner, *Can. Med. Assoc. J.*, 2005, **172**, 1039–1043.
17 J. Gaffney, S. Matou-Nasri, M. Grau-Olivares and M. Slevin, *Mol. BioSyst.*, 2010, **6**, 437–443.
18 U. Anderegg, J. C. Simon and M. Averbeck, *Exp. Dermatol.*, 2014, **23**, 295–303.
19 K. A. Gutowski, *Clin. Plast. Surg.*, 2016, **43**, 489–496.
20 M. Kong, X. G. Chen, D. K. Kweon and H. J. Park, *Carbohydr. Polym.*, 2011, **86**, 837–843.
21 J.-M. Song, J.-H. Im, J.-H. Kang and D.-J. Kang, *Carbohydr. Polym.*, 2009, **78**, 633–634.
22 P. Kongtawelert and P. Ghosh, *Anal. Biochem.*, 1989, **178**, 367–372.
23 S. Pepeliaev, R. Hrudíková, J. Jílková, J. Pavlík, D. Smirnou, Z. Černý and L. Franke, *Eur. Polym. J.*, 2017, **94**, 460–470.
24 K. Yang, M. Liu, Y. Wang, S. Wang, H. Miao, L. Yang and X. Yang, *Sens. Actuators, B*, 2017, **251**, 503–508.
25 J. R. M. Martins, C. C. Passerotti, R. M. B. Maciel, L. O. Sampaio, C. P. Dietrich and H. B. Nader, *Anal. Biochem.*, 2003, **319**, 65–72.
26 H. Q. Luo, N. B. Li and S. P. Liu, *Biosens. Bioelectron.*, 2006, **21**, 1186–1194.
27 N. Oueslati, P. Leblanc, C. Harscoat-Schiavo, E. Rondags, S. Meunier, R. Kapel and I. Marc, *Carbohydr. Polym.*, 2014, **112**, 102–108.
28 Y.-H. Chen and Q. Wang, *Carbohydr. Polym.*, 2009, **78**, 178–181.
29 K. Ruckmani, S. Z. Shaikh, P. Khalil, M. S. Muneera and O. A. Thusleem, *J. Pharm. Anal.*, 2013, **3**, 324–329.
30 U. Resch-Genger, M. Grabolle, S. Cavaliere-Jaricot, R. Nitschke and T. Nann, *Nat. Methods*, 2008, **5**, 763.
31 J. M. Costa-Fernández, R. Pereiro and A. Sanz-Medel, *TrAC, Trends Anal. Chem.*, 2006, **25**, 207–218.
32 H. F. Wang, Y. Y. Wu and X. P. Yan, *Anal. Chem.*, 2013, **85**, 1920–1925.
33 G. Tang, L. Du and X. Su, *Food Chem.*, 2013, **141**, 4060–4065.
34 D. M. Willard, L. L. Carillo, J. Jung and A. V. Orden, *Nano Lett.*, 2001, **1**, 469–474.
35 S. Gupta, T. Smith, A. Banaszak and J. Boeckl, *Nanomaterials*, 2017, **7**, 301.
36 P. Hui, L. Zhang, T. H. M. Kjällman, A. Christian Soeller and J. Travassejdic, *J. Am. Chem. Soc.*, 2007, **129**, 3048–3049.
37 Y. Miao, *RSC Adv.*, 2015, **5**, 76804–76812.
38 Y. Miao, M. Yang and G. Yan, *RSC Adv.*, 2016, **6**, 8588–8593.
39 P. Wu, Y. He, H. F. Wang and X. P. Yan, *Anal. Chem.*, 2010, **82**, 1427–1433.
40 Z. Zhang, Y. Miao, Q. Zhang, L. Lian and G. Yan, *Biosens. Bioelectron.*, 2015, **68**, 556.
41 Y. Wei, H. Li, H. Hao, Y. Chen, C. Dong and G. Wang, *Polym. Chem.*, 2015, **6**, 591–598.
42 D. Zhu, W. Li, H.-M. Wen, Q. Chen, L. Ma and Y. Hu, *Anal. Methods*, 2014, **6**, 7489–7495.
43 J. Lv, Y. Miao and G. Yan, *RSC Adv.*, 2017, **7**, 41063–41069.
44 J. Zhuang, X. Zhang, G. Wang, D. Li, W. Yang and T. Li, *J. Mater. Chem.*, 2003, **13**, 1853–1857.
45 I. Yildiz, M. Tomasulo and F. M. Raymo, *Proc. Natl. Acad. Sci. U. S. A.*, 2006, **103**, 11457–11460.
46 J. H. Chung, C. S. A. And and D. J. Jang, *J. Phys. Chem. B*, 2001, **105**, 4128–4132.
47 O. Kulakovich, N. Strekal, A. Yaroshevich, S. Maskevich, S. Gaponenko, I. Nabiev, A. Ulrike Woggon and M. Artemyev, *Nano Lett.*, 2002, **2**, 1449–1452.